Breaking the Ring of Fire: How ridge collision, slab age, and convergence rate narrowed and terminated the Antarctic continental arc

Alex Burton-Johnson[a], Joaquin Bastias[b,c], Stefan Kraus[d]

[a]British Antarctic Survey, High Cross, Madingley Road, Cambridge, CB3 0ET, UK
[b]Department of Geology, Trinity College Dublin, Dublin 2, Ireland
[c]Carrera Geología, Facultad de Ingeniería, Universidad Andres Bello, Sazie 2119, Santiago, Chile
[d]CDM Smith SE, Fuerther Str. 232, 90429 Nuremberg

Correspondence to: Alex Burton-Johnson (alerto@bas.ac.uk)

Key Points

- New $^{40}Ar/^{39}Ar$ ages from the South Shetland Islands show the youngest outcrops of Antarctic arc magmatism were emplaced at ~20–19 Ma.
- The Antarctic Peninsula continental arc narrowed through the Cenozoic due to the subduction of progressively younger oceanic crust.
- Steepening slab dip beneath the South Shetland Islands narrowed and migrated the final magmatic activity offshore.

Abstract. The geometry of the Antarctic-Phoenix Plate system, with the Antarctic Plate forming both the overriding plate and the conjugate to the subducting oceanic plate, allows quantification of slab age and convergence rate back to the Paleocene and direct comparison with the associated magmatic arc. New Ar-Ar data from Cape Melville (South Shetland Islands, SSI) and collated geochronology shows Antarctic arc magmatism ceased at ~19 Ma. Since the Cretaceous, the arc front remained ~100 km from the trench whilst its rear migrated trenchward at 6 km/Myr. South of the SSI, arc magmatism ceased ~8–5 Myr prior to each ridge-trench collision, whilst on the SSI (where no collision occurred) the end of arc magmatism predates the end of subduction by ~16 Myr. Despite the narrowing and successive cessation of the arc, geochemical and dyke orientation data shows the arc remained in a consistently transitional state of compressional continental arc and extensional backarc tectonics. Numerically relating slab age, convergence rate, and slab dip to the Antarctic-Phoenix Plate system, we conclude that the narrowing of the arc and the cessation of magmatism south of the South Shetland Islands was primarily in response to the subduction of progressively younger oceanic crust, and secondarily to the decreasing convergence rate. Increased slab dip beneath the SSI migrated the final magmatism offshore. Comparable changes in the geometry and composition are observed on the Andean arc, suggesting slab age and convergence rate may affect magmatic arc geometry and composition in settings currently attributed to slab dip variation.

1. Introduction

Arc magmatism is reliant on the volatile flux derived from the subducting oceanic crust. If this flux is disturbed, magmatism can cease. The arrival of a spreading ridge at a subduction zone can provide such terminations or pauses in magmatism (Sisson et al., 2003), but understanding the timing and processes associated with the end of arc magmatism requires a suitable geological record. Such a record is found on the Antarctic Peninsula, where progressive ridge-trench collisions terminated a long-lived continental arc. However, if arc magmatism is a product of the volatile flux from active subduction then an anomaly arises, for arc magmatism ceased on the Antarctic Peninsula at ~19 Ma despite subduction continuing until 3.3 Ma (Jin et al., 2009; Livermore et al., 2000). This study evaluates field, geochemical, and geochronological data to determine the timing and cause of arc cessation, and the relation to regional tectonics. We collect new data from Cape Melville on King George Island (South Shetland Islands), where prior work reported the youngest outcrops of Antarctic arc magmatic rocks; compile the regional data to evaluate how the magmatism and tectonic deformation changed as arc cessation approached; and finally compare our observations with the Andean magmatic arc to evaluate whether our conclusions from the Antarctic Peninsula are more broadly applicable.

1.1. Geological background

The Antarctic Peninsula developed as an autochthonous continental arc on the margin of the Gondwanan supercontinent (Burton-Johnson & Riley, 2015). Seafloor spreading between New Zealand and Antarctica along what is now the Pacific-Antarctic ridge commenced at ~84 Ma (Mortimer et al., 2019), following an extended period of pre-breakup rifting and magmatism of Gondwana through the Late Cretaceous (~101–82 Ma; Tulloch et al., 2009). Subsequent seafloor spreading generated oceanic crust of the Pacific Plate to the NW, and the Antarctic Plate to the SE. Along the NW margin of the Antarctic Peninsula, subduction of the Phoenix Plate (also referred to in the literature as the “Aluk” or “Drake” Plate) beneath the Peninsula continued synchronously with continued seafloor spreading along the Antarctic-Phoenix ridge; a divergent plate boundary initiated at the DeGerlache Magnetic Anomaly during a South Pacific plate reorganisation and ridge-jump event at ~61 Ma (Cande et al., 1995; McCarron & Larter, 1998). With the same Antarctic Plate now forming the conjugate oceanic crust to the NW, and the overriding continental crust to the SE, the Antarctic-Phoenix spreading ridge migrated towards the continental margin with consequently equal rates of spreading and convergence. Ultimately, this ridge migration collided successive segments of the spreading centre with the continental margin. With each ridge-trench collision, subduction ceased progressively northwards along the Antarctic Peninsula through the Cenozoic (Larter & Barker, 1991), until ridge-trench collision south of the Hero Fracture Zone at 3.3 ±0.2 Ma resulted in the termination of oceanic spreading and the end of Phoenix Plate subduction (Jin et al., 2009; Larter & Barker, 1991; Livermore et al., 2000). Subsequent sinistral simple-shear between the Antarctic and Scotia plates led to opening of the Bransfield Basin as a pull-apart basin (an extension of the South Scotia Ridge Fault), developing contractional structures in the margin South Shetland Trench as the transtensional rifting forcefully migrated the South Shetland Islands to the NW (Fretzdorff et al., 2004; González-Casado et al., 2000; Jin et al., 2009).

With the progressive northwards cessation of subduction, arc magmatism also ceased progressively northwards, finally ending in the South Shetland Islands at ~20 Ma (Birkenmajer et al., 1985) (Fig. 1). After ~10 Myr, regional magmatism resumed as low-volume alkaline magmatism, including that associated with the opening of the Bransfield Strait (Fig. 1; Smellie, 1987; Košler et al., 2009). Contemporaneously, extension between South America and Antarctica and

back-arc extension of the Scotia subduction zone developed a deep water connection in the Drake Passage at 34-30 Ma (Eagles et al., 2006); initiating the Antarctic Circumpolar Current.

However, this history fails to explain: 1) why arc magmatism largely ceased at 20 Ma, despite subduction continuing to ~3.3 Ma; 2) why subsequent magmatism has alkaline compositions associated with intraplate magmatism; and 3) why there is a >10 Myr interval between arc and intra-plate magmatism.

1.2. Problems with the existing hypothesis

Barker (1982) identified a ~50–60 Myr delay between the youngest magmatic ages aligned with each fracture zone-bounded ocean segment and the collision age of the associated ridge segment. They compared this with the collision of the Pacific-Kula Ridge and the Aleutian Arc (DeLong et al., 1978), where a 15 Myr magmatic hiatus was observed either side of the ~30 Ma ridge collision (i.e. 45–15 Ma). Assuming a 45° slab dip, DeLong et al. (1978) proposed that magmatism ceased when ocean floor younger than 25–30 Myr was at a depth of 100 km beneath the arc. Barker (1982) noted a similar relationship on the Antarctic Peninsula, proposing that the cessation of arc magmatism resulted from a decrease in dehydration depth as progressively younger oceanic crust was subducted. They proposed this was in response to the *"earlier escape of bound water because of the higher temperature, less continuous sediment cover and more fractured and permeable nature of the younger oceanic crust"*.

However, Byrne (1979) subsequently concluded that the Pacific-Kula Ridge ceased spreading in the Late Paleocene (~59–56 Ma), challenging the previously proposed Oligocene (~35–30 Ma) ridge subduction model (DeLong et al., 1978). Consequently, the plate motions of the North Pacific continue under discussion (Domeier et al., 2017; Vaes et al., 2019), and as such we cannot constrain the Antarctic processes using the Aleutian Arc. Instead, we should recognise that the Antarctic Peninsula system is a unique opportunity to inform on processes elsewhere, as the history of self-subduction, well-constrained marine magnetic anomalies, and terrestrial magmatic ages constrain the plate motions, crustal ages, and magmatic activity through the Cenozoic.

Collating the current geochronological dataset (Fig. 1; data compilation in Supplementary Material), an interval of only ~5–8 Myr of non-magmatic subduction occurred on the Antarctic Peninsula south of the Anvers Fracture Zone; much less than the ~50–60 Myr interval proposed by Barker (1982). However, ~17 Myr did occur between the final calc-alkaline arc magmatism of the South Shetland Islands and the 3.3 Ma ridge-trench collision. Whilst a significantly shorter duration than that identified by Barker (1982), this is over twice the duration of amagmatic subduction interval farther south.

Present day magmatic gaps exist along the Pacific subduction zone of North and South America (Siebert & Simkin, 2002), but the oldest subducting oceanic crust adjacent to these magmatic gaps is ~10 Myr old: 6.6 Ma at the Juan de Fuca-Pacific intersection (Currie & Riddihough, 1982), 9.7 Ma at the Rivera-Pacific intersection (Lonsdale, 1991), 13.1 Ma at the Cocos-Nazca intersection (Lonsdale, 2005), and 8.9 Ma at the Antarctic-Nazca intersection (Tebbens et al., 1997). Arc magmatism on the Antarctic Peninsula would thus be expected to continue until ~10 Myr prior to ridge-trench collision. This is true for the Antarctic Peninsula ridge-trench collisions at 14.5 Ma and older (Fig. 1) but not the ~17 Myr of amagmatic subduction on the South Shetland Islands. Is the age of the subducting ocean crust responsible, as proposed by Barker (1982), or are other processes in control?

1.3. Constraining the end of Antarctic magmatism

To understand the relationship between subduction and the end of magmatism we must constrain the timing and origin of the final arc magmatism. Previous work indicated this occurred on King George Island (KGI, Fig. 1), where a Cretaceous to Early Miocene volcanic arc sequence is overlain by <2.7 Ma alkaline volcanics (Birkenmajer, 1996; Pańczyk & Nawrocki, 2011). Following revision of an anomalous 14.4 Ma K-Ar volcanic age (Birkenmajer et al., 1986) to 23.7 Ma by Ar-Ar geochronology (Smellie et al., 1998), the only evidence for <20 Ma arc magmatism in the northern Antarctic Peninsula is a set of NW-SE striking dykes at Cape Melville on the eastern end of KGI (19.9 ±0.3 and 20.1 ±0.2 Ma, K-Ar; Birkenmajer et al., 1985), crosscut by younger undated NE-SW striking dykes (proposed to be Late Pliocene to Early Pleistocene) (Fig. 2). This paper revisits the Cape Melville magmatism, evaluating its origins via field relations, geochronology, and geochemistry, and then compares the Cenozoic magmatic and marine magnetic data to evaluate the tectonic and magmatic history that led to the end of Antarctic arc magmatism.

2. Methods

2.1. $^{40}Ar/^{39}Ar$ geochronology

Samples from the basaltic dykes of Cape Melville on King George Island in the South Shetland Islands were collected in 2019 aboard the *HMS Protector* for $^{40}Ar/^{39}Ar$ geochronology and geochemistry (Fig. 2) and analysed at Open University, UK. For $^{40}Ar/^{39}Ar$ dating, samples were powdered then sieved and washed repeatedly in de-ionised water. Alteration-free whole rock pieces were cleaned ultrasonically in acetone and de-ionised water, dried, and irradiated at the McMaster Nuclear Reactor (McMaster University, Canada) for 102 hours. Neutron flux was monitored using biotite mineral standard GA1550 (99.738 ± 0.104 Ma; Renne et al., 2011). The irradiated samples were loaded into an ultra-high vacuum system and a 1059nm CSI fibre laser was focussed into the sample chamber to step-heat the basalt. Extracted gases were cleaned for 5 minutes using two SAES AP-10 getters, one running at 450°C and one at room temperature, following which the gases were let into a MAP 215-50 mass spectrometer for measurement. The mass discrimination value was measured at 283 for $^{40}Ar/^{36}Ar$ (using a calibration noble gas mixture of known composition). System blanks were measured before and after every one or two sample analyses. Gas clean-up and inlet is fully automated, with measurement of ^{40}Ar, ^{39}Ar, ^{38}Ar, ^{37}Ar, and ^{36}Ar, each for ten scans, and the final measurements are extrapolations back to the inlet time.

The system blanks measured before and after every one or two sample analyses were subtracted from the raw sample data. Results were corrected for ^{37}Ar and ^{39}Ar decay, and neutron-induced interference reactions. The following correction factors were used: $(^{39}Ar/^{37}Ar)Ca = 0.00065\pm0.00000325$, $(36Ar/37Ar)Ca = 0.000265\pm0.000001325$, and $(40Ar/39Ar)K = 0.0085\pm0.0000425$; based on analyses of Ca and K salts. Ages were calculated using the atmospheric 40Ar/36Ar ratio of 298.56 (Lee et al., 2006) and decay constants of Renne et al. (2011). All data corrections were carried out using an Excel macro and ages were calculated using Isoplot 4.15 (Ludwig, 2012). All ages are reported at the 2σ level and include a 0.5% error on the J value. Plateau criteria of at least 50% of the ^{39}Ar release in at least 3 consecutive steps were used. Analytical data are included in the Supplementary Material.

2.2. Geochemistry

The Cape Melville basaltic dyke samples were analysed by inductively coupled plasma optical emission spectrometry (ICP-OES) and inductively coupled plasma-mass spectrometry (ICP-MS) by Chemostrat (Welshpool, UK). The

samples were prepared using the $LiBO_2$ fusion procedure (Jarvis & Jarvis, 1992). Separate aliquots of the prepared samples were analysed using a ThermoFisher iCAP ICP-OES and ThermoFisher X-Series II ICP-MS instruments. Major elements are reported in weight % oxide form and trace elements in parts per million (data in Supplementary Material).

3. Results

3.1. $^{40}Ar/^{39}Ar$ geochronology

Step-heating of sample B18.20.1 (the NE-striking dyke) produced a slightly sloping plot with a $^{40}Ar/^{39}Ar$ plateau age of 23.3 ±1.1 Ma (MSWD = 1.4; Fig. 3). This plateau age contains over the 50% threshold of ^{39}Ar release required for a valid plateau age, but the plot shows older and younger ages at the low and higher temperature steps, indicating some disturbance to the Ar system. The inverse isochron (Fig. 3) produces a younger age (19.0 ±1.0 Ma) than the plateau. B18.24.1 (the NW-striking dyke) gives a $^{40}Ar/^{39}Ar$ plateau age of 21.5 ± 0.4 Ma (MSWD = 0.8; Fig. 3). This plateau age contains 58.4% of the ^{39}Ar release, from a release spectra that slopes from older apparent ages in the initial steps to younger in the final steps. The inverse isochron correlation plot of the data from this step heat (Fig. 3) calculates an age of 20.7 ±0.6 Ma.

The $^{40}Ar/^{36}Ar$ intercept of the inverse isochrons for both samples are above the atmospheric ratio (assumed to be 298.56), suggesting that there may be excess argon in the sample. This likely results in the older apparent ages seen in the initial steps of the release spectra, although the excess argon can be present in plateau steps as well. Consequently, the inverse isochron age (which makes no assumptions of the atmospheric ratio) may be considered the best age estimate.

3.2. Geochemistry

The Cape Melville dykes are all basaltic or marginally basaltic andesite in composition. The key chemical distinction between the two dyke species is that the NW-striking dykes are tholeiite series, whilst the NE-striking dykes are alkaline (Fig. 4a). Primitive mantle multi-element plots for the dykes (Fig. 4b) show the LILE and LREE enrichment and HFSE and HREE depletions characteristic of arc magmatism. The Ti-Zr-Y tectonic discrimination for basalts classifies the NW-striking dykes as continental arc basalts, whilst the NE-striking dykes display the transitional MORB to island arc tholeiite chemistry associated with suprasubduction zone, marginal backarc basin magmatism (Fig. 4c).

3. Discussion

3.1. When did arc magmatism cease?

Previously published K-Ar ages and field relationships indicated that the Cape Melville dykes represented the youngest arc magmatism in Antarctica: ~20 Ma for the NW-SE striking dykes, and younger undated (but proposed to be Late Pliocene to Early Pleistocene) NE-SW striking dykes crosscutting them (Birkenmajer et al., 1985). Our new Ar-Ar geochronology indicates that both dyke sets were emplaced at ~20 Ma: 19.0 ±1.0 Ma for the NE-striking dykes, and 20.7 ±0.6 Ma for the NW-striking dyke. These Ar-Ar ages are supported by the 22.6 ±0.4 Ma Rb-Sr age for fossils of the country rock (Dingle & Lavelle, 1998). However, field evidence shows the NE-striking dykes to be cross-cut by

the NW-striking dykes (Fig. 3); more aligned with the relative ages of the $^{40}Ar/^{39}Ar$ plateaux: 23.3 ±1.1 Ma for the NE-striking dykes, and 21.5 ± 0.4 Ma for the NW-striking dyke (Fig. 3). Considering both the field relations and the evidence for excess argon affecting the plateaux ages thus indicates that whilst the inverse isochron ages are a more accurate estimate of the emplacement age (~21–19 Ma rather than the older ~23–21 Ma estimate of the plateaux), the relative ages and error estimates are incorrect. Either way, there is no longer evidence on the Antarctic Peninsula for <19 Ma arc magmatism.

Comparing the new and compiled magmatic ages with their distance from the continent-ocean boundary (COB, Fig. 5a) shows a distinctly linear relationship in the distribution of the arc since the Late Cretaceous (data compilation in Supplementary Material). However, rather than simply migrating towards the trench, the arc progressively narrowed with the arc front remaining 100–150 km from the COB, whilst the most distal arc magmatism migrated towards the trench at a steady 6 km/Myr until arc cessation at ~19 Ma. Over this period, the magmatism became more primitive in its $^{143}Nd/^{144}Nd$ isotopic composition relative to mantle compositions at the time (Fig. 5b and Fig. 5c). Collating data from South America (Supplementary Material), similar but slower (2 km/Myr) narrowing of the Andean continental arc can be observed between ~350–100 Ma, although it subsequently widened again at 11 km/Myr between ~70–20 Ma (Fig. 5e). The period of arc-narrowing was also associated with progressively more primitive $^{143}Nd/^{144}Nd$ isotopic compositions, with a return to more evolved isotopes in the subsequent period of arc-widening (Fig. 5f and Fig. 5g).

3.2. What drove the cessation of Antarctic magmatism?

3.2.1. Tectonic setting

Applying tectonic discrimination diagrams to the new and previously-published geochemical and geochronological data for the Antarctic Peninsula shows that arc magmatism continued until ~19 Ma, whilst all subsequent magmatism was intraplate in composition (Fig. 6). The basaltic/gabbroic data (Fig. 6a and Fig. 6b) show this transition clearly, with only minor intraplate basaltic magmatism prior to ~19 Ma. Ti-Zr-Y tectonic discrimination shows that the magmatism ranged from continental arc basalts to transitional, backarc magmatism since the Late Cretaceous (Fig. 6c). Only after 10 Ma (with occasional exceptions) did magmatism switch from dominantly subduction-derived to wholly intraplate. The rhyolitic/granitic data indicates more occurrences of intraplate magmatism, but the multiple pathways of assimilation and fractional crystallisation by which felsic rocks can be derived renders this discrimination more ambiguous.

In addition to their chemistry, dyke orientations can also be used to constrain the syn-magmatic tectonic setting and allow identification of changes in the syn-magmatic strain regime that may have affected the end of arc magmatism. When a dyke intrudes by active hydraulic fracturing through isotropic crust, it strikes in the direction of maximum lateral compression (Anderson, 1951; Hubbert & Willis, 1957). Whilst this is most commonly the case, dyke orientation is also affected by local pre-existing crustal weaknesses, preferentially emplacing into reactivated pre-existing planar discontinuities close to parallel to the main shortening axis (e.g. faults, joints, and shear zones) (Sielfeld et al., 2017). This commonly involves dyke emplacement into pre-existing and reactivated joint systems and strike-slip faults (Bird, 2002; Kraus et al., 2010; Spacapan et al., 2016), with the strike of conjugate strike-slip faults typically developing at ~30° either side of the direction of maximum compression (the angle of internal friction; Anderson, 1951; Borg & Handin, 1966). Thus, if we can constrain the subduction convergence direction, we can predict orientations of dykes emplaced either by hydraulic fracturing (i.e. parallel to the maximum shortening) or by

reactivating pre-existing strike slip faults (i.e. ~30° oblique to the maximum shortening direction) in response to subduction-driven compression or extension (Fig. 7).

As the youngest subduction was almost perfectly perpendicular to the continental margin (and thus parallel to the fracture zones; Larter and Barker, 1991), we can infer from the fracture zones offshore of the South Shetland Islands that final subduction convergence was oriented at ~130°. This is identical to the 128° subduction convergence direction inferred from chrons C27–C24 (61–53 Ma) of the marine magnetic anomalies (McCarron & Larter, 1998). We can thus conclude that subduction convergence was SE-oriented at ~130° throughout the Cenozoic. This orientation is parallel to the strike of the NW-striking dykes of Cape Melville, and perpendicular to its NE-striking dykes, and matches the predicted dyke orientations under hydraulic fracturing for Fig. 7a and Fig. 7b. Therefore, the NW-striking continental arc dykes on Cape Melville were emplaced by hydraulic fracturing during subduction-perpendicular crustal shortening (compression), whilst the NE-striking, backarc dykes were emplaced during subduction-perpendicular crustal extension. As noted above, Ti-Zr-Y tectonic discrimination of the Cape Melville dykes (Fig. 4c) showed both continental arc (NW-striking dykes) and marginal backarc basin chemistries (NE-striking dykes). The inferred deformation regime is thus in agreement with the geochemically-inferred tectonic settings. As both dyke sets were emplaced at ~20–19 Ma, this transition in strain regime and resultant magmatic character occurred quickly (<2 Myr).

In this way, we can evaluate the dyke orientations of the broader South Shetland Islands since the Cretaceous. Compiled dyke orientations and geochronology (Fig. 8a) by this study and previous publications (Kraus et al., 2008, 2010; Kraus, 2005) show that, as on Cape Melville, orthogonal sets of dyke orientations (both parallel and perpendicular to the continental margin) emplaced by hydraulic fracturing under subduction-driven compression and extension have been the dominant emplacement mechanism since 50 Ma (Fig. 8b, Fig. 8d, and Fig. 8e). However, between 70–50 Ma, both clusters of dyke orientations were oblique to the subduction convergence direction (Fig. 8f). Instead, they closely resemble the predicted orientations of dykes emplaced within extensional strike-slip faults (Fig. 7d). This is supported by the displacement on sheared dykes and faults recorded by Kraus et al. (2010), with one population of conjugate shear structures (70–100° dextral and 140–164° sinistral displacement) matching that predicted for compressional deformation (Fig. 7c), and another population of conjugate structures (1–17° dextral and 45–79° sinistral displacement) matching that predicted for extensional deformation (Fig. 7d); these latter orientations resembling those of the 70–50 Ma dykes (Fig. 8f). We can conclude that between 70–50 Ma, the South Shetland Islands were dominantly under suprasubduction extension.

Magmatism on the South Shetland Islands peaked between 50–40 Ma (Fig. 8g). Dyke orientations show both extension and compression during this period, although NW-SE directed compression was dominant (Fig. 8b and Fig. 8e). The magmatic flux reduced again after 40 Ma (Fig. 8g), with both NW-SE directed compression and extension recorded by the 30–18 Ma dykes. Geochemical discrimination (Fig. 6c) shows that magmatism on the broader Antarctic Peninsula ranged from continental arc basalts to transitional, backarc magmatism since the Late Cretaceous, only switching from dominantly subduction-derived to wholly intraplate after 10 Ma. The dyke orientations and basaltic chemistry thus imply that the tectonic setting remained in a consistently transitional state of compressional continental arc and extensional backarc tectonics from the Late Cretaceous to the Early Miocene, with no singular shift in setting to explain the end of arc magmatism.

3.2.2. Slab age and/or convergence rate

The dyke chemistry and orientations of the South Shetland Islands indicate that there was no progressive change in tectonic setting to explain the end of arc magmatism prior to the end of subduction. Based on comparison with the

Aleutian Arc and its collision with the Kula Ridge, Barker (1982) proposed that the arrival of oceanic crust younger than ~30–25 Myr at 100 km depth beneath the Antarctic continental arc led to a ~60–50 Myr interval between the end of magmatism and the end of subduction. However, as noted above, the Kula Ridge spreading ceased ~29–21 Myr earlier than previously understood, and we have revised the ~60–50 Myr interval identified by Barker (1982) to only ~20–10 Myr. Whether the subduction of progressively younger crust can explain the end of Antarctic arc magmatism thus needs revaluation.

Offshore marine magnetic anomalies (Cande et al., 1982, 1995; Eagles, 2003; Eagles et al., 2004; Eagles & Scott, 2014; Larter et al., 2002; Larter & Barker, 1991; Wobbe et al., 2012) provide exceptional temporal and spatial constraints on the age and spreading rates of the Antarctic and Phoenix ocean crust. This data shows that spreading rates on the Antarctic-Phoenix ridge decreased rapidly between ~60–40 Ma (particularly dramatically at 52.3 Ma; McCarron & Larter, 1998), remaining subsequently consistently slow until the cessation of rifting. Although subduction was sub-perpendicular to the continental margin through much of the Cenozoic, the Late Cretaceous spreading ridge continued laterally to the DeGerlache Gravity Anomaly (1000 km NW of Alexander Island; Larter et al., 2002). This geometry would have imparted a dextral obliquity and clockwise rotation to the earlier subduction history, and thus reduced the earlier convergence rate for a given spreading rate and increased the subduction rate farther from the rotation pole (i.e. faster subduction beneath the South Shetland Islands than farther south along the Peninsula). By generating and rotating synthetic isochrons for the conjugate (now subducted) Phoenix Plate to the preserved Antarctic Plate in GPlates (Fig. 10h, Boyden et al., 2011), we can simulate the rotation and convergence history of the Phoenix Plate back to 61 Ma (GPlates files included in Supplementary Material) and calculate the convergence history at different points along the Antarctic Peninsula. This modelled convergence (Fig. 5d) shows the fast (~200 km/Myr) Paleocene subduction of the Phoenix Plate, its rapid diminishment in the Eocene, and the subsequent consistently slow (~70–35 km/Myr) subduction until the Pliocene cessation of Antarctic-Phoenix Ridge spreading.

Our new and compiled geochronological data shows that from the Late Cretaceous until its ~19 Ma magmatic cessation, the Antarctic Peninsula continental arc narrowed at a rate of 6 km/Myr (Fig. 5a). Although other processes may enhance magmatic activity (e.g. tectonic deformation), the generation of calc-alkaline arc magmas by partial melting of the mantle is principally a result of volatile addition from the subducting slab (Grove et al., 2012). By numerically modelling the thermo-mechanical and thermodynamic processes involved in slab dehydration, Magni et al. (2014) showed that fast, old slabs remain hydrated until deeper in the mantle than slow, young slabs. This is because older slabs are colder, most importantly in the mantle lithosphere at their core where water is stored in serpentine. Consequently, faster and/or older subducting ocean crust hydrates the mantle over a wider area, and so should be associated with wider magmatic arcs. Inversely, slower and/or younger slabs should be associated with narrower arcs.

The onset and cessation depth of slab dehydration was calculated by Magni et al. (2014) for various slab ages and convergence rates (albeit at a constant 30° slab dip). From these results, a relationship between the onset and cessation depths and the thermal parameter $\Phi = av_s \sin(\theta)$ can be observed (Kirby et al., 1991), where a is the age of the subducting slab (Myr), v_s is the convergence rate (km/Myr), θ is the slab dip (°), and Φ has units km. Plotting their results, we have derived empirical relationships for the onset (linear) and cessation (logarithmic) depths of slab dehydration (Fig. 9).

These empirical relationships enable us to explore the effects of convergence rate, slab age, and slab dip on the width of the Antarctic magmatic arc. As noted above, convergence rate was calculated by generating and rotating synthetic isochrons for the conjugate Phoenix Plate using the observed magnetic isochrons of the Antarctic Plate (Fig. 10h). These synthetic isochrons and derived Phoenix Plate rotation enabled the slab age at the trench to be estimated over

time. For the South Shetland Islands, these isochrons were extended further back using the synthetic isochrons of the crust to the south (Fig. 10h). Because of the distribution of Antarctic isochrons, for the earlier stages of Phoenix subduction we can estimate the convergence rate but not the slab age at the trench. Furthermore, the slab age at the trench levels off further back in time, for these earlier periods the oldest calculable slab age at the trench is used as a constant value for the modelled ages preceding it (see Fig. 10b and Fig. 10e). However, as the Antarctic-Phoenix spreading ridge originated at the DeGerlache Gravity Anomaly at ~61 Ma, possibly via a ridge-jump event (McCarron & Larter, 1998), the true slab ages preceding the oldest calculable age are ambiguous.

From the synthetic isochrons and plate rotations, for each 1 Myr the convergence rate and the age of the crust at different depths and distances (for a constant but modifiable slab dip) could be calculated. From these values, we compute the thermal parameter, Φ, the onset and cessation depths of slab dehydration, and the equivalent horizontal distances from the trench. The calculations were executed in two stages. Firstly, an assumed distance (200 km) between the trench and the arc was used for which the time for the subducting slab to reach vertically beneath this distance estimate, and its age when it did so, could be calculated at each 1 Myr. The second stage instead used the horizontal distance estimates of the first stage. In this way, the slab age and resultant depths at the start and end of dehydration could be calculated whilst being invariant to the first distance estimate.

Using this approach, we simulated the horizontal slab dehydration window for two locations (Fig. 10h): Point A (66° S, 65° W) between the South Anvers and Biscoe fracture zones, where subduction ceased between 15.0–14.1 Ma (Larter et al., 1997), and Point B (62.5° S, 59.5° W) in the South Shetland Islands, where subduction ceased at 3.3 Ma (Livermore et al., 2000).

For Point A, the magnetic anomalies enable us to estimate slab dehydration between ~59–15 Ma. For a 40° slab dip, the onset of slab dehydration would have occurred consistently at ~100 km from the trench (Fig. 10c; a comparable distance to the observed magmatic activity) until 17 Ma (at which time the subducted slab was 4 Myr old when it commenced dehydration). Although subduction ceased at 14.5 Ma, insufficient crust entered the trench from 16 Ma onwards to begin dehydration. Whilst the estimated onset of slab dehydration remained ~100 km from the trench, the horizontal distance between the trench and vertically above the cessation depth of slab dehydration narrowed from ~300 km to ~100 km between ~59–17 Ma, again closely agreeing with the observed magmatic age compilation (Fig. 10c). Magni et al. (2014) found that the onset of dehydration was principally affected by the subduction velocity, whilst the end depth of dehydration was dominantly affected by the age of the slab. Consequently, it is principally the steadily younging slab ages shown in Fig. 10b that narrow the magmatic arc at Point A and farther south on the Antarctic Peninsula.

As noted above, by extending the synthetic isochrons for the subducted Phoenix crust beneath Point B, we can estimate the slab dehydration window between ~60–4 Ma. For a 40° slab dip, the onset of dehydration again occurs beneath ~100 km from the trench; again, in agreement with the magmatic data. From ~7 Ma onwards, insufficient crust is subducted to reach dehydration depths, hence the end of the slab dehydration window at 8 Ma; 5 Myr prior to the end of subduction. However, unlike Point A, ridge-trench collision did not occur offshore of Point B. As such, the age of the slab at the end of its dehydration remains between ~40–30 Myr throughout the period the model predicts dehydration to occur. Consequently, unlike at Point A, we would not expect the narrowing of the arc, nor the observed 20 Ma interval between the end of arc magmatism on the South Shetland Islands and the end of subduction.

Using the parameters above, we would not expect arc magmatism to cease simultaneously at Points A and B. One variable we have not discussed is the effect of slab dip on the distribution of magmatism. 40° is optimal to simulate the changing width of the magmatic arc south of the South Shetland Islands. However, observed slab dips around the

world are highly variable even at shallow depths, ranging from ~45°–10° (average of 23°) in the upper 100 km to ~70°–10° (average of 49°) between 200–100 km depth (Hu & Gurnis, 2020). Whilst it may seem intuitive that older, colder slabs subduct with a steeper dip, no direct function has been found between slab age and slab dip (Cruciani et al., 2005; Jarrard, 1986). In fact, younger slabs may be found to have steeper dips (Hu & Gurnis, 2020). Slab age is thus one of many contributing factors, with longer-lived subduction zones, lower slab descent velocities, wider subduction zones, and continental rather than oceanic overriding plates all being associated with shallower dip angles of the subducting slab (Cruciani et al., 2005; Hu & Gurnis, 2020; Jarrard, 1986; Schellart, 2020).

We propose therefore that following collision of the Antarctic-Phoenix Ridge south of the Anvers fracture zone, the slab dip steepened from~40° to >60° in response to the drastic narrowing of the subduction zone. Modelling this change in slab dip (Fig. 10g) shows this would have reduced the horizontal distance between the trench and the window of slab dehydration, migrating the arc offshore of the South Shetland Islands until its eventual estimated cessation at 8 Ma. This steepening of the slab dip is supported by the identification of a steeply-dipping (~70°) high-velocity anomaly at 100–300 km beneath the northernmost Antarctic Peninsula, interpreted to be the subducted Phoenix Plate (Park et al., 2012). However, variable slab dip cannot explain the narrowing of the magmatic arc farther south, as the observed distribution of magmatic activity indicates that the arc front remained a constant distance from the trench, unlike the distances predicted by modelling variable dip (Fig. 10g). The narrowing of the arc is thus primarily in response to the subduction of progressively younger oceanic crust.

3.3. Comparison with the Andean continental arc

Our compilation of Andean magmatism shows comparable trends to the Antarctic Peninsula (Fig. 5), with progressive narrowing of the subduction zone between 350–100 Ma and subsequent widening between 70–20 Ma. As for the Antarctic Peninsula, the narrower the Andean arc, the more primitive and narrower its range of $^{143}Nd/^{144}Nd$ isotopic compositions (Fig. 5); indicative of lower assimilation of the overriding plate. That the data shows arc “widening” is significant, as Andean literature instead describes arc “migration” (e.g. Kay et al., 2005; Mamani et al., 2010; Chapman et al., 2017; Oliveros et al., 2020). This has led prior studies to invoke changes in the slab dip (Oliveros et al., 2020), which primarily affects the arc location rather than its width (Fig. 10g). The lack of a complete plate circuit between the Pacific Ocean plates and their continental margins prior to 83 Ma prevents earlier estimation of plate convergence rates. However, using GPlates and the plate rotations of Matthews et al. (2016), we can calculate the Farallon-South America Plate convergence for 20° S, 70° W from 83 Ma onwards (Fig. 5h). This shows an increase in convergence rate from ~55–20 Ma, synchronous with ~500 km of arc widening. Unlike the simple geometry of the Antarctic-Phoenix subduction system, the multiple plates and spreading ridges associated with the Pacific and the Farallon-South America subduction system prevent accurate estimation of slab age at the trench prior to ~15 Ma and thus prevent modelling of the system as we have the Antarctic Peninsula. However, given the similar magmatic distributions and chemistries of the Antarctic Peninsula and the Andes, and the apparent relationship between plate convergence rate and width of the Andean arc, we propose that convergence rate and slab age were also primary controls on the width of Andean magmatism since the Carboniferous.

Conclusions

Following revision of the youngest outcrops of arc magmatism on the Antarctic Peninsula, we conclude that the Antarctic arc ceased to be active at ~20–19 Ma, with the youngest dyke activity of Cape Melville on King George Island (South Shetland Islands) yielding inverse Ar-Ar isochron ages of 19.0 (±1.0 Ma) and 20.7 (±0.6 Ma) (Fig. 3).

Collated into a revised geochronology compilation, we see that Antarctic Peninsula arc magmatism ceased 5–8 Myr prior to each successive ridge trench collision, with each collision progressively marking the end of Phoenix Plate subduction beneath Antarctica. However, ridge-trench collision did not occur offshore of the South Shetland Islands (the northernmost end of the Peninsula). Here, a ~16 Myr interval occurred between the end of arc magmatism and the end of subduction; significantly longer than the interval observed farther south, or along other arcs (Fig. 1).

Compiled geochemical and dyke orientation data shows no change in the tectonic setting to explain this discrepancy during the progressive cessation of arc magmatism (Fig. 6 and Fig. 8). Instead, the arc remained in a consistently transitional state of compressional continental arc and extensional backarc tectonics from the Late Cretaceous to the Early Miocene. What did change was the arc width and its crustal assimilation (evidenced by compiled geochronology and $^{143}Nd/^{144}Nd$ isotopes) (Fig. 5). From the Cretaceous until ~20 Ma, the arc front remained ~100 km from the trench whilst its rear migrated trenchward at 6 km/Myr. During this, the magmatic $^{143}Nd/^{144}Nd$ isotopes became more juvenile in composition, indicating lower rates of crustal assimilation. We collated the marine magnetic anomalies and generated synthetic conjugate isochrons in GPlates, constraining the ages and convergence rates of the subducting Phoenix Plate through time. By calculating and applying the numerically-deduced relationships between slab age, convergence rate, and slab dip to the Antarctic-Phoenix Plate system (Fig. 10), we conclude that the narrowing of the arc and the cessation of magmatism south of the South Shetland Islands was primarily in response to the subduction of progressively younger oceanic crust, and to a lesser extent the decreasing convergence rate. However, this should not have led to narrowing of the magmatic arc or its synchronous ~20–19 Ma cessation on the South Shetland Islands, as no ridge-trench collision or crustal younging occurred prior to 10 Ma. Instead, based on our calculations, we propose that following the sudden narrowing of the subduction zone following the adjacent ridge-trench collisions, the slab dip increased to >60°, migrating the remaining activity offshore until its estimated cessation at ~8 Ma (Fig. 10).

Due to its geometry, with the Antarctic Plate forming both the overriding plate and the conjugate to the subducting oceanic plate, the Antarctic-Phoenix system uniquely allows quantification of slab age and convergence rate back to the Paleocene. However, its narrowing and isotopically-changing arc is comparable elsewhere. Most notably, the Andean arc progressively narrowed and developed more primitive Nd isotopes between 350–100 Ma, before widening and returning to less primitive compositions contemporaneously with an increase in convergence rate (Fig. 5). Whilst slab dip variation is singularly invoked to explain such changes there and elsewhere, this should migrate rather than narrow the arc. Consequently, although slab age and convergence rate are not always as quantifiable as on the Antarctic Peninsula, we suggest they are more common controls on magmatic arc geometry and composition than currently recognised.

Acknowledgements

All analytical data for the geochemistry and $^{40}Ar/^{39}Ar$ geochronology of the Cape Melville dykes are included in the Supplementary Material. We thank the Royal Navy ship, *HMS Protector* for fieldwork support. This study is part of the British Antarctic Survey Polar Science for Planet Earth programme, funded by the Natural Environment Research Council. $^{40}Ar/^{39}Ar$ analyses were funded by the Trans-Antarctic Association. Thanks to Alison Halton and Sarah Sherlock at Open University for conducting the $^{40}Ar/^{39}Ar$ analyses, to Valentina Magni for discussions on numerical modelling and subduction zone dynamics, and to Rob Larter for comments on our manuscript. Joaquín Bastías was funded by the Instituto Antártico Chileno (INACH, project RT-06-14) and the Swiss National Science Foundation (project P500PN_202847).

418

419 **References**

420 Amante, C., & Eakins, B. W. (2009). ETOPO1 Arc-Minute Global Relief Model: Procedures, Data Sources and
421 Analysis, National Oceanic and Atmospheric Administration Technical Memorandum NESDIS NGDC-24.

422 Anderson, E. M. (1951). The dynamics of faulting and dyke formation with applications to Britain. Oliver and Boyd.

423 Barker, P. F. (1982). The Cenozoic subduction history of the Pacific margin of the Antarctic Peninsula: ridge crest–
424 trench interactions. Journal of the Geological Society, 139(6), 787–801.

425 Bird, P. (2002). Stress direction history of the western United States and Mexico since 85 Ma. Tectonics, 21(3), 5–1.

426 Birkenmajer, K. (1996). Polish geological research on King George Island, West Antarctica (1977-1996). Pol. Polar
427 Res, 17(3–4), 125–141.

428 Birkenmajer, K., Gazdzicki, A., Kreuzer, H., & Müller, P. (1985). K–Ar Dating of the Melville Glaciation (Early
429 Miocene). West Antarctica: Polish Academy of Sciences, Bulletin, Earth Sciences, 33, 15–23.

430 Birkenmajer, K., Delitala, M. C., Narebski, W., Nicoletti, M., & Petrucciani, C. (1986). Geochronology of Tertiary
431 island-arc volcanics and glacigenic deposits, King George Island, South Shetland Islands (West Antarctica).
432 Bulletin of the Polish Academy of Sciences. Earth Sciences, 34(3), 257–273.

433 Birkenmajer, K., Soliani, E., & Kawashita, K. (1988). Early Miocene K-Ar Age of Volcanic Basement of the Melville
434 Glaciation Deposits, King George Island, West Antarctica. Bulletin of the Polish Academy of Sciences. Earth
435 Sciences, 36(1), 25–34.

436 Borg, I., & Handin, J. (1966). Experimental deformation of crystalline rocks. Tectonophysics, 3(4), 249–367.

437 Boyden, J. A., Müller, R. D., Gurnis, M., Torsvik, T. H., Clark, J. A., Turner, M., et al. (2011). Next-generation plate-
438 tectonic reconstructions using GPlates. In G. R. Keller & C. Baru (Eds.), Geoinformatics: Cyberinfrastructure
439 for the Solid Earth Sciences (pp. 95–113). Cambridge University Press.

440 Burton-Johnson, A., & Riley, T. R. (2015). Autochthonous v. accreted terrane development of continental margins: a
441 revised in situ tectonic history of the Antarctic Peninsula. Journal of the Geological Society, 172(6), 822–
442 835.

443 Byrne, T. (1979). Late Paleocene demise of the Kula-Pacific spreading center. Geology, 7(7), 341–344.

444 Cande, S. C., Herron, E. M., & Hall, B. R. (1982). The early Cenozoic tectonic history of the southeast Pacific. Earth
445 and Planetary Science Letters, 57(1), 63–74.

446 Cande, S. C., Raymond, C. A., Stock, J., & Haxby, W. F. (1995). Geophysics of the Pitman Fracture Zone and Pacific-
447 Antarctic plate motions during the Cenozoic. Science, 270(5238), 947–953.

Chapman, J. B., Ducea, M. N., Kapp, P., Gehrels, G. E., & DeCelles, P. G. (2017). Spatial and temporal radiogenic isotopic trends of magmatism in Cordilleran orogens. Gondwana Research, 48, 189–204.

Cruciani, C., Carminati, E., & Doglioni, C. (2005). Slab dip vs. lithosphere age: no direct function. Earth and Planetary Science Letters, 238(3–4), 298–310.

Currie, R. G., & Riddihough, R. P. (1982). Geophysical surveys in Northeast Pacific. AAPG Bulletin, 66(7), 963.

DeLong, S. E., Fox, P. J., & McDowell, F. W. (1978). Subduction of the Kula ridge at the Aleutian trench. Geological Society of America Bulletin, 89(1), 83–95.

Dingle, R. V., & Lavelle, M. (1998). Antarctic Peninsular cryosphere: Early Oligocene (c. 30 Ma) initiation and a revised glacial chronology. Journal of the Geological Society, 155(3), 433–437.

Domeier, M., Shephard, G. E., Jakob, J., Gaina, C., Doubrovine, P. V., & Torsvik, T. H. (2017). Intraoceanic subduction spanned the Pacific in the Late Cretaceous–Paleocene. Science Advances, 3(11), eaao2303.

Eagles, G. (2003). Tectonic evolution of the Antarctic–Phoenix plate system since 15 Ma. Earth and Planetary Science Letters, 217(1–2), 97–109.

Eagles, G., & Scott, B. G. (2014). Plate convergence west of Patagonia and the Antarctic Peninsula since 61 Ma. Global and Planetary Change, 123, 189–198.

Eagles, G., Gohl, K., & Larter, R. D. (2004). Life of the Bellingshausen plate. Geophysical Research Letters, 31(7).

Eagles, G., Livermore, R., & Morris, P. (2006). Small basins in the Scotia Sea: the Eocene Drake passage gateway. Earth and Planetary Science Letters, 242(3–4), 343–353.

Fretzdorff, S., Worthington, T. J., Haase, K. M., Hékinian, R., Franz, L., Keller, R. A., & Stoffers, P. (2004). Magmatism in the Bransfield basin: rifting of the South Shetland Arc? Journal of Geophysical Research: Solid Earth, 109(B12).

González-Casado, J. M., Robles, J. L. G., & López-Martínez, J. (2000). Bransfield Basin, Antarctic Peninsula: not a normal backarc basin. Geology, 28(11), 1043–1046.

Grove, T. L., Till, C. B., & Krawczynski, M. J. (2012). The role of H2O in subduction zone magmatism. Annual Review of Earth and Planetary Sciences, 40, 413–439.

Hu, J., & Gurnis, M. (2020). Subduction duration and slab dip. Geochemistry, Geophysics, Geosystems, 21(4), e2019GC008862.

Hubbert, M. K., & Willis, D. G. (1957). Mechanics of hydraulic fracturing. Transactions of the AIME, 210(01), 153–168.

Irvine, T. N. J., & Baragar, W. R. A. (1971). A guide to the chemical classification of the common volcanic rocks. Canadian Journal of Earth Sciences, 8(5), 523–548.

Jarrard, R. D. (1986). Relations among subduction parameters. Reviews of Geophysics, 24(2), 217–284.

Jarvis, I., & Jarvis, K. E. (1992). Plasma spectrometry in the earth sciences: techniques, applications and future trends. Chemical Geology, 95(1–2), 1–33.

Jin, Y. K., Lee, J., Hong, J. K., & Nam, S. H. (2009). Is subduction ongoing in the South Shetland Trench, Antarctic Peninsula?: new constraints from crustal structures of outer trench wall. Geosciences Journal, 13(1), 59–67.

Kay, S. M., Godoy, E., & Kurtz, A. (2005). Episodic arc migration, crustal thickening, subduction erosion, and magmatism in the south-central Andes. Geological Society of America Bulletin, 117(1–2), 67–88.

Kirby, S. H., Durham, W. B., & Stern, L. A. (1991). Mantle phase changes and deep-earthquake faulting in subducting lithosphere. Science, 252(5003), 216–225.

Košler, J., Magna, T., Mlčoch, B., Mixa, P., Nỳvlt, D., & Holub, F. V. (2009). Combined Sr, Nd, Pb and Li isotope geochemistry of alkaline lavas from northern James Ross Island (Antarctic Peninsula) and implications for back-arc magma formation. Chemical Geology, 258(3), 207–218.

Kraus, S. (2005). Magmatic dyke systems of the South Shetland Islands volcanic arc (West Antarctica): reflections of the geodynamic history (PhD Thesis). LMU Munich: Faculty of Geosciences, München. Retrieved from http://resolving.de/urn:nbn:de:bvb:19-38277

Kraus, S., Miller, H., Dimov, D., Hegner, E., McWilliams, M., & Pecskay, Z. (2008). Structural geology of the Mesozoic Miers bluff formation and crosscutting Paleogene dikes (Livingston Island, South Shetland Islands, Antarctica) – insights into the geodynamic history of the northern Antarctic peninsula. Journal of South American Earth Sciences, 26(4), 498–512.

Kraus, S., Poblete, F., & Arriagada, C. (2010). Dike systems and their volcanic host rocks on King George Island, Antarctica: Implications on the geodynamic history based on a multidisciplinary approach. Tectonophysics, 495(3–4), 269–297.

Larter, R. D., & Barker, P. F. (1991). Effects of ridge crest-trench interaction on Antarctic-Phoenix Spreading: Forces on a young subducting plate. Journal of Geophysical Research: Solid Earth, 96(B12), 19583–19607.

Larter, R. D., Rebesco, M., Vanneste, L. E., Gamboa, L. A. P., & Barker, P. F. (1997). Cenozoic tectonic, sedimentary and glacial history of the continental shelf west of Graham Land, Antarctic Peninsula. Wiley Online Library. Retrieved from http://onlinelibrary.wiley.com/doi/10.1029/AR071p0001/summary

Larter, R. D., Cunningham, A. P., Barker, P. F., Gohl, K., & Nitsche, F. O. (2002). Tectonic evolution of the Pacific margin of Antarctica 1. Late Cretaceous tectonic reconstructions. Journal of Geophysical Research: Solid Earth (1978–2012), 107(B12), EPM-5.

Le Maitre, R. W., Bateman, P., Dudek, A., Keller, J., Lameyre Le Bas, M. J., Sabine, P. A., et al. (1989). A classification of igneous rocks and glossary of terms. Oxford: Blackwell Publishing.

Lee, J.-Y., Marti, K., Severinghaus, J. P., Kawamura, K., Yoo, H.-S., Lee, J. B., & Kim, J. S. (2006). A redetermination of the isotopic abundances of atmospheric Ar. Geochimica et Cosmochimica Acta, 70(17), 4507–4512.

Livermore, R., Balanyá, J. C., Maldonado, A., Martínez, J. M., Rodríguez-Fernández, J., de Galdeano, C. S., et al. (2000). Autopsy on a dead spreading center: the Phoenix Ridge, Drake Passage, Antarctica. Geology, 28(7), 607–610.

Lonsdale, P. (1991). Structural Patterns of the Pacific Floor Offshore of Peninsular California: Chapter 7: Part III. Regional Geophysics and Geology.

Lonsdale, P. (2005). Creation of the Cocos and Nazca plates by fission of the Farallon plate. Tectonophysics, 404(3–4), 237–264.

Ludwig, K. R. (2012). User's manual for Isoplot 3.75: A geochronological toolkit for Microsoft Excel. Berkeley, California.

Magni, V., Bouilhol, P., & Van Hunen, J. (2014). Deep water recycling through time. Geochemistry, Geophysics, Geosystems, 15(11), 4203–4216.

Mamani, M., Wörner, G., & Sempere, T. (2010). Geochemical variations in igneous rocks of the Central Andean orocline (13 S to 18 S): Tracing crustal thickening and magma generation through time and space. Bulletin, 122(1–2), 162–182.

Matthews, K. J., Maloney, K. T., Zahirovic, S., Williams, S. E., Seton, M., & Mueller, R. D. (2016). Global plate boundary evolution and kinematics since the late Paleozoic. Global and Planetary Change, 146, 226–250.

McCarron, J. J., & Larter, R. D. (1998). Late Cretaceous to early Tertiary subduction history of the Antarctic Peninsula. Journal of the Geological Society, 155(2), 255–268.

Mortimer, N., van den Bogaard, P., Hoernle, K., Timm, C., Gans, P. B., Werner, R., & Riefstahl, F. (2019). Late Cretaceous oceanic plate reorganization and the breakup of Zealandia and Gondwana. Gondwana Research, 65, 31–42.

Oliveros, V., Vásquez, P., Creixell, C., Lucassen, F., Ducea, M. N., Ciocca, I., et al. (2020). Lithospheric evolution of the Pre-and Early Andean convergent margin, Chile. Gondwana Research, 80, 202–227.

Pańczyk, M., & Nawrocki, J. (2011). Pliocene age of the oldest basaltic rocks of Penguin Island (South Shetland Islands, northern Antarctic Peninsula). Geological Quarterly, 55(4), 335–344.

Park, Y., Kim, K.-H., Lee, J., Yoo, H. J., & Plasencia L, M. P. (2012). P-wave velocity structure beneath the northern Antarctic Peninsula: evidence of a steeply subducting slab and a deep-rooted low-velocity anomaly beneath the central Bransfield Basin. Geophysical Journal International, 191(3), 932–938.

Pearce, J. A. (1982). Trace element characteristics of lavas from destructive plate boundaries. In R. S. Thorpe (Ed.), Andesites (pp. 525–548). Chichester, UK: Wiley.

Pearce, J. A., & Cann, J. R. (1973). Tectonic setting of basic volcanic rocks determined using trace element analyses. Earth and Planetary Science Letters, 19(2), 290–300.

Pearce, J. A., Harris, N. B. W., & Tindle, a. G. (1984). Trace Element Discrimination Diagrams for the Tectonic Interpretation of Granitic Rocks. Journal of Petrology, 25(4), 956–983. https://doi.org/10.1093/petrology/25.4.956

Renne, P. R., Balco, G., Ludwig, K. R., Mundil, R., & Min, K. (2011). Response to the comment by WH Schwarz et al. on "Joint determination of 40K decay constants and 40Ar∗/40K for the Fish Canyon sanidine standard, and improved accuracy for 40Ar/39Ar geochronology" by PR Renne et al.(2010). Geochimica et Cosmochimica Acta, 75(17), 5097–5100.

Schellart, W. P. (2020). Control of subduction zone age and size on flat slab subduction. Frontiers in Earth Science, 8, 26.

Siebert, L., & Simkin, T. (2002). Volcanoes of the world: An illustrated catalog of holocene volcanoes and their eruptions (Global Volcanism Program Digital Information Series No. GVP-3). Washington D.C., USA: Smithsonian Institution. Retrieved from https://volcano.si.edu/

Sielfeld, G., Cembrano, J., & Lara, L. (2017). Transtension driving volcano-edifice anatomy: Insights from Andean transverse-to-the-orogen tectonic domains. Quaternary International, 438, 33–49.

Sisson, V. B., Pavlis, T. L., Roeske, S. M., & Thorkelson, D. J. (2003). Introduction: An overview of ridge-trench interactions in modern and ancient settings. Geological Society of America Special Papers, 371, 1–18.

Smellie, J. L. (1987). Geochemistry and tectonic setting of alkaline volcanic rocks in the Antarctic Peninsula: a review. Journal of Volcanology and Geothermal Research, 32(1), 269–285.

Smellie, J. L., Millar, I. L., Rex, D. C., & Butterworth, P. J. (1998). Subaqueous, basaltic lava dome and carapace breccia on King George island, South Shetland Islands, Antarctica. Bulletin of Volcanology, 59(4), 245–261.

Spacapan, J. B., Galland, O., Leanza, H. A., & Planke, S. (2016). Control of strike-slip fault on dyke emplacement and morphology. Journal of the Geological Society, 173(4), 573–576.

Sun, S. -s., & McDonough, W. F. (1989). Chemical and isotopic systematics of oceanic basalts: implications for mantle composition and processes. Geological Society, London, Special Publications, 42(1), 313–345. https://doi.org/10.1144/GSL.SP.1989.042.01.19

Tebbens, S. F., Cande, S. C., Kovacs, L., Parra, J. C., LaBrecque, J. L., & Vergara, H. (1997). The Chile ridge: A tectonic framework. Journal of Geophysical Research: Solid Earth, 102(B6), 12035–12059.

Tulloch, A. J., Ramezani, J., Kimbrough, D. L., Faure, K., & Allibone, A. H. (2009). U-Pb geochronology of mid-Paleozoic plutonism in western New Zealand: Implications for S-type granite generation and growth of the east Gondwana margin. Geological Society of America Bulletin, B26272-1.

Vaes, B., van Hinsbergen, D. J., & Boschman, L. M. (2019). Reconstruction of subduction and back-arc spreading in the NW Pacific and Aleutian Basin: clues to causes of Cretaceous and Eocene plate reorganizations. Tectonics.

Wobbe, F., Gohl, K., Chambord, A., & Sutherland, R. (2012). Structure and breakup history of the rifted margin of West Antarctica in relation to Cretaceous separation from Zealandia and Bellingshausen plate motion. Geochemistry, Geophysics, Geosystems, 13(4).

582 **Figures**

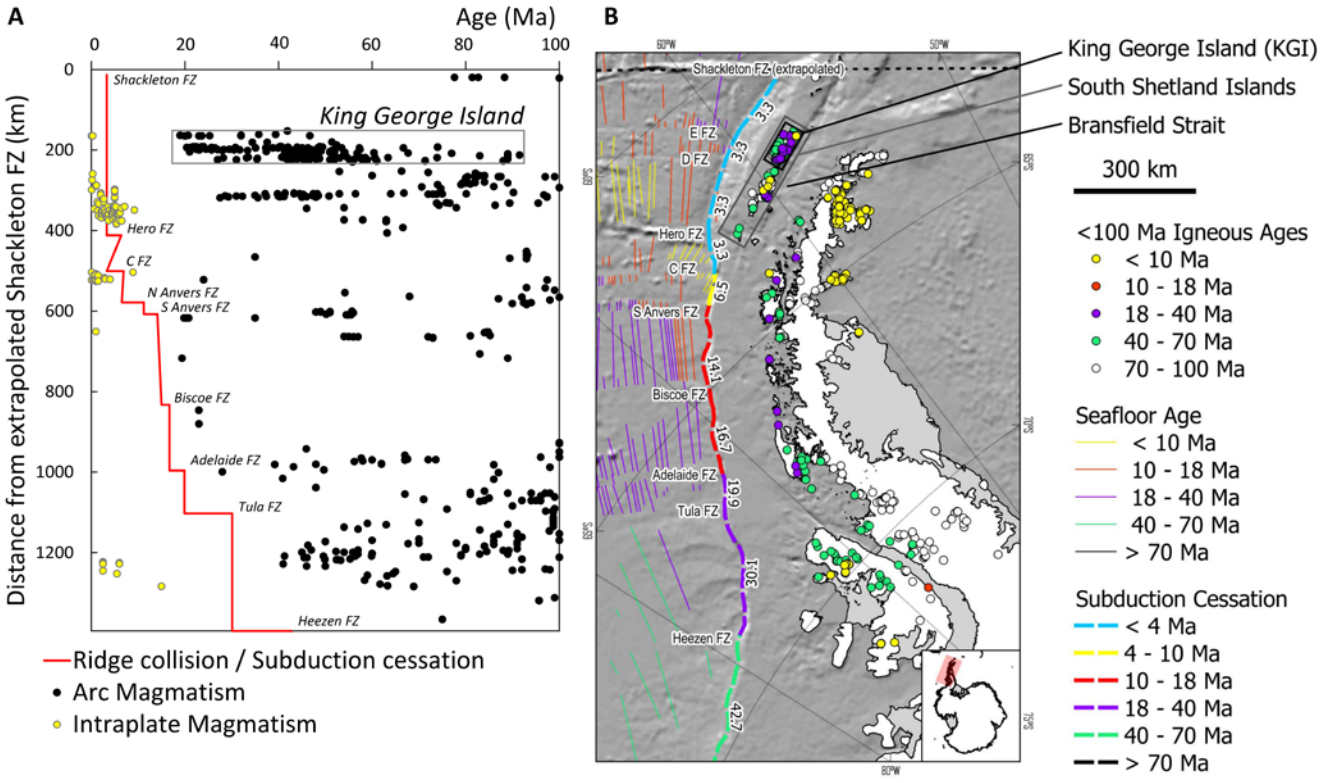

583

584 **Fig. 1.**

585 Magmatic history of the Antarctic Peninsula. A) Temporal and spatial plot of magmatism and the history of ridge
586 collisions and subduction cessation on the Antarctic Peninsula (Larter et al., 1997). B) Temporal and spatial map of
587 Antarctic Peninsula magmatism, subduction cessation (ages labelled; Larter et al., 1997; Livermore et al., 2000), and
588 offshore magnetic anomalies. Magmatic age compilation included in Supplementary Material.
589 Bathymetry from ETOPO1 (Amante & Eakins, 2009).

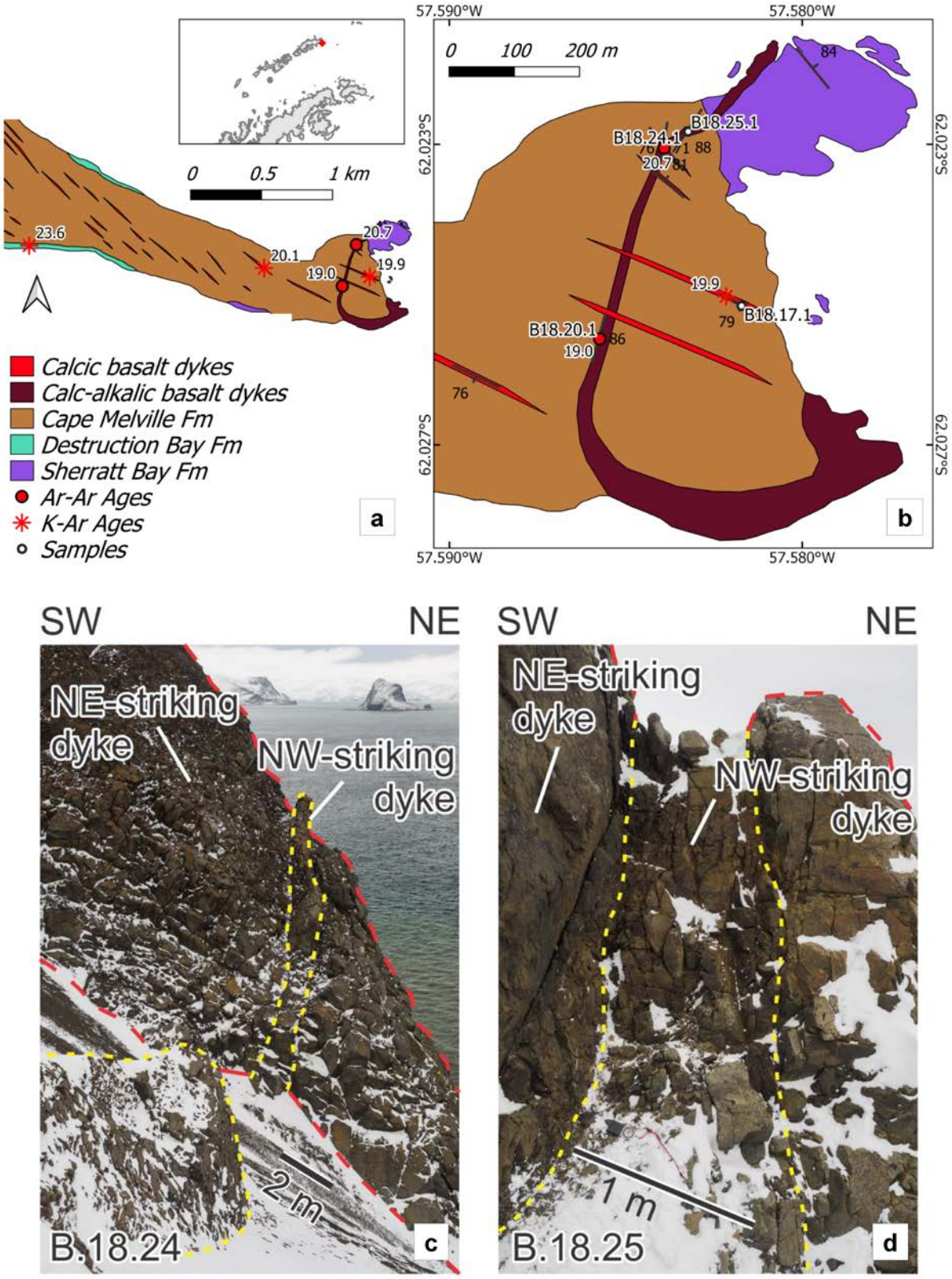

590

591 **Fig. 2.**

592 a) and b) Revised geological map of Cape Melville (modified from Birkenmajer et al., 1985). Sample locations and
593 dyke orientations shown. $^{40}Ar/^{39}Ar$ ages from this study. K-Ar ages from Birkenmajer et al. (1985, 1988). c) and d)
594 Intersections of the two dyke species at Cape Melville. At both outcrops, different NW-striking dykes (outlined in
595 yellow) crosscut the same NE-striking dyke (outlined in red). Site location IDs in Fig. 2b.

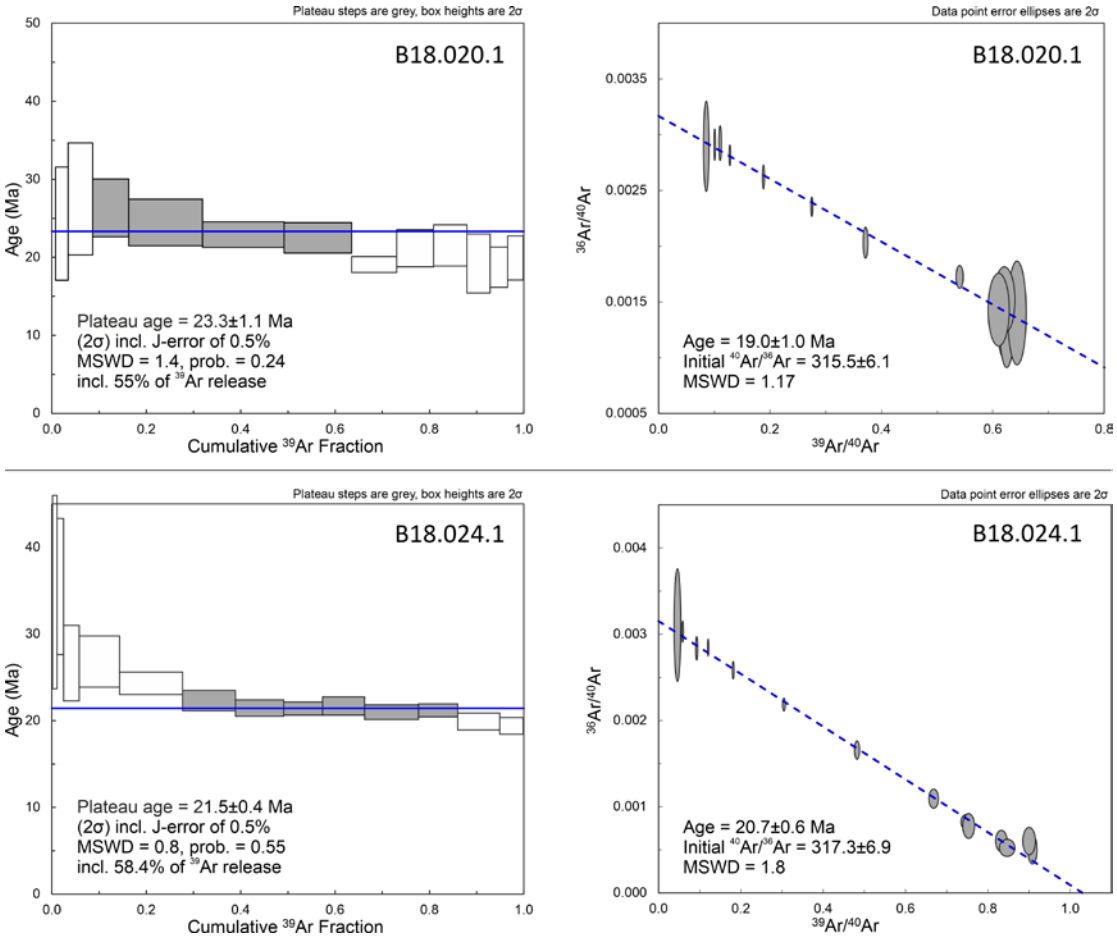

Fig. 3.

$^{40}Ar/^{39}Ar$ data for the NE-striking (B18.020.1) and NW-striking (B18.024.1) mafic dykes of Cape Melville. The $^{40}Ar/^{36}Ar$ isochron intercepts are above atmospheric values, suggesting there may be excess argon present. This may result in the older apparent ages seen in the initial steps of the release spectra, but may also be present in plateau steps. For this reason, the inverse isochron age may be considered the best estimate for the age of this sample. However, the relative isochron ages between the two dykes are at odds with the apparent field relations, whilst the plateau ages are not.

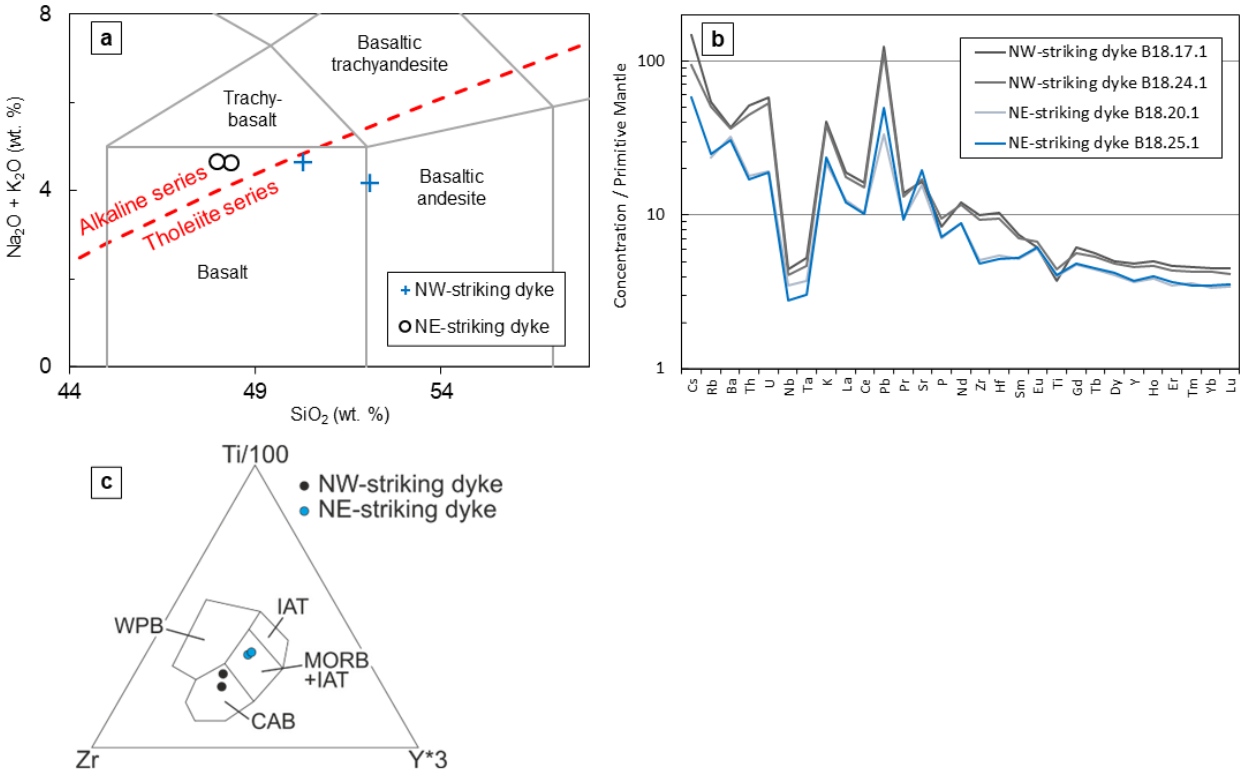

605

606 **Fig. 4.**

607 a–c) Geochemistry of the Cape Melville basaltic dykes. a) Total alkali-silica (TAS, Le Maitre et al., 1989) and alkaline-
608 tholeiite discrimination (Irvine & Baragar, 1971). b) Multi-element, primitive mantle normalised trace element plots.
609 Normalising values from Sun and McDonough (1989). c) Ti-Zr-Y tectonic discrimination diagram of basaltic rocks
610 (Pearce & Cann, 1973). WPB – Within Plate Basalt; IAT – Island Arc Tholeiite; MORB; Mid-Ocean Ridge Basalt;
611 CAB – Continental Arc Basalt.

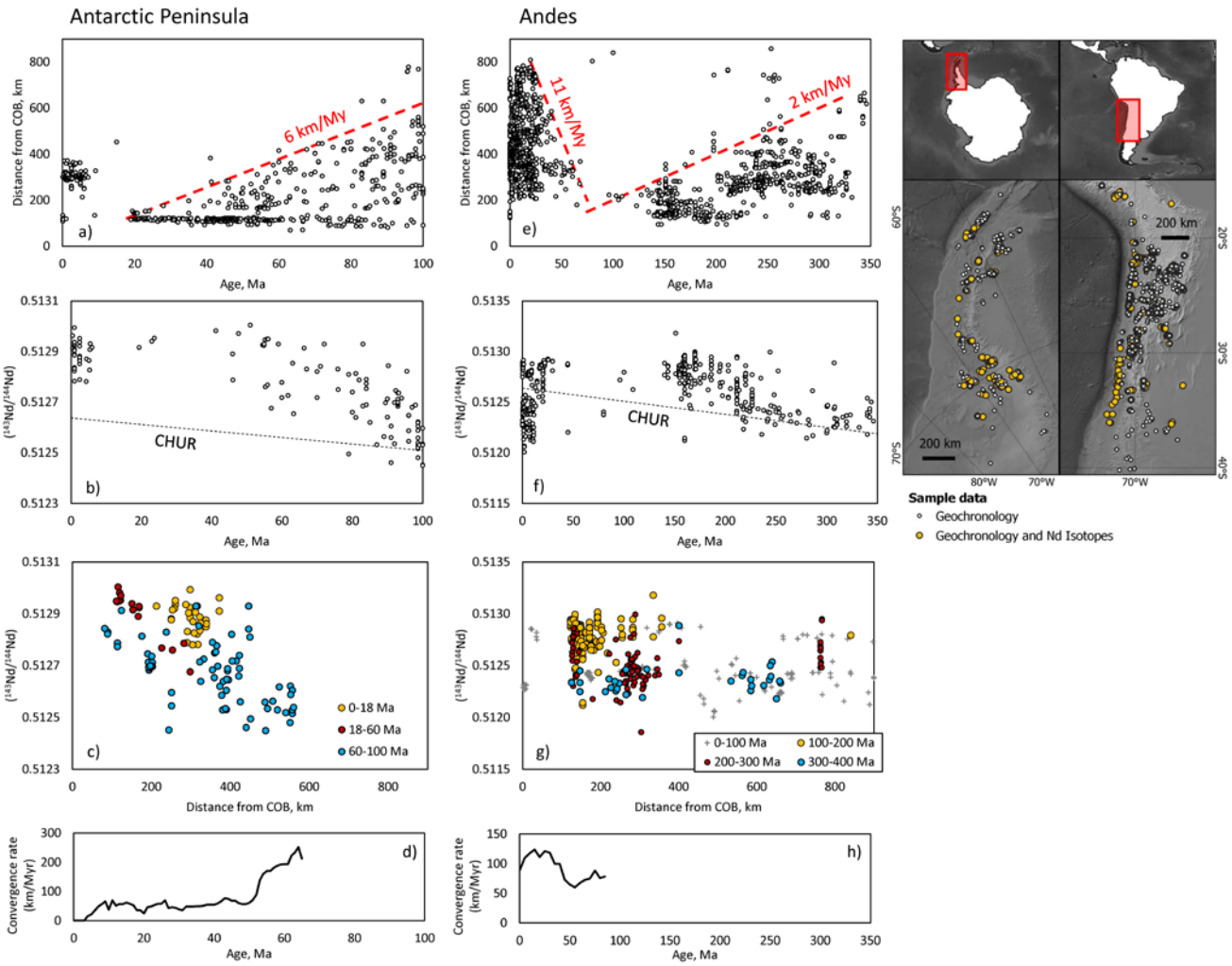

612

613 **Fig. 5.**

614 Comparison of magmatic age, distance from the continent-ocean boundary (COB), and $^{143}Nd/^{144}Nd$ isotopic
615 compositions for the Antarctic Peninsula and Andean continental arcs (Supplementary Material; Mamani et al., 2010;
616 Chapman et al., 2017; Oliveros et al., 2020, and the Geochemistry of Rocks of the Oceans and Continents database
617 (GEOROC), http://georoc.mpch-mainz.gwdg.de). Antarctic-Phoenix Plate convergence calculated in GPlates (Boyden
618 et al., 2011) for 62.5° S, 59.5° W using Matthews et al. (2016) for Pacific and Antarctic Plate rotation, and tracing and
619 rotating synthetic isochrons for the conjugate (now subducted) Phoenix Plate to the preserved Antarctic Plate magnetic
620 anomalies. Farallon-South America Plate convergence calculated for 20° S, 70° W using the rotations of Matthews et
621 al. (2016).

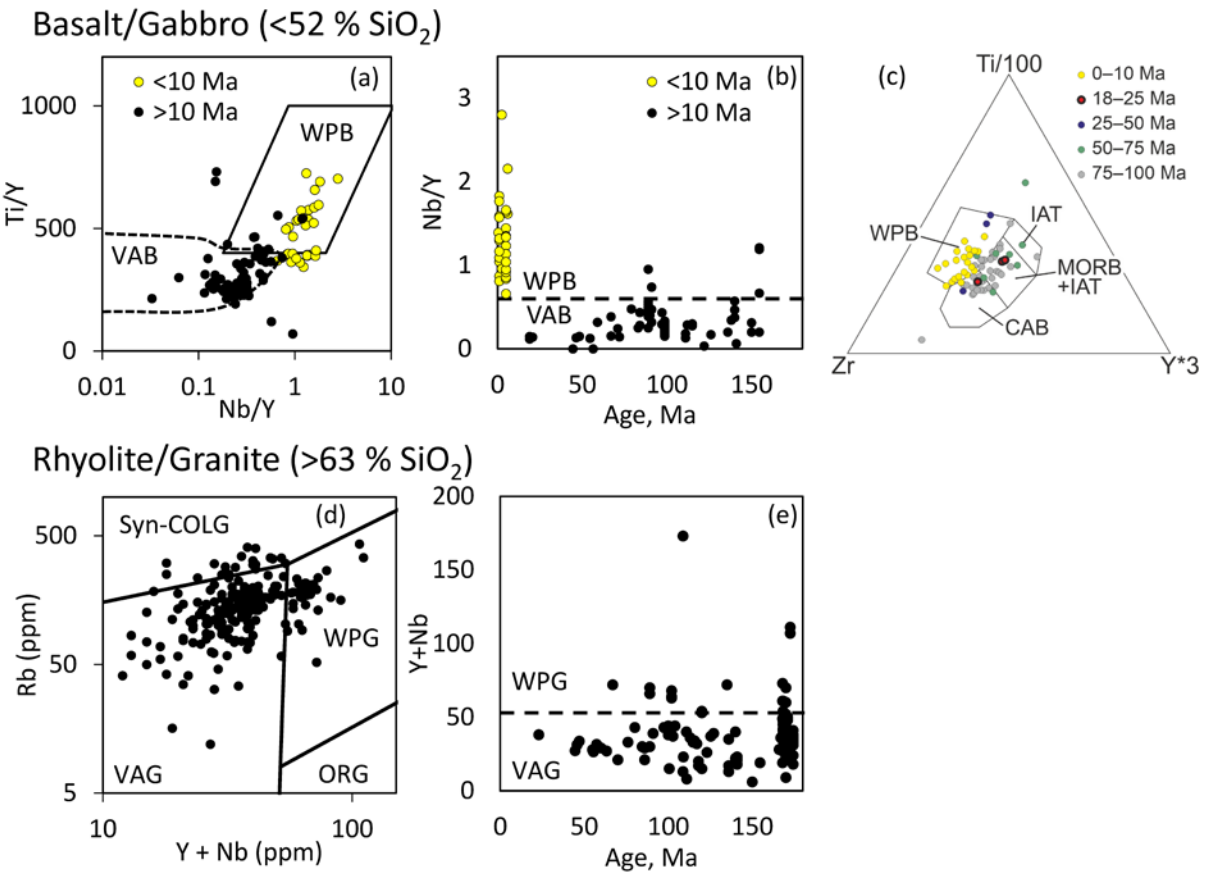

622

623 **Fig. 6.**

624 Basaltic (a–c) and rhyolitic (d and e) tectonic discrimination diagrams for Antarctic Peninsula magmatism showing
625 the consistent continental arc setting until <10 Ma. Tectonic discrimination diagrams and discrimination values from
626 Pearce & Cann (1973), Pearce (1982), and Pearce et al. (1984)

627

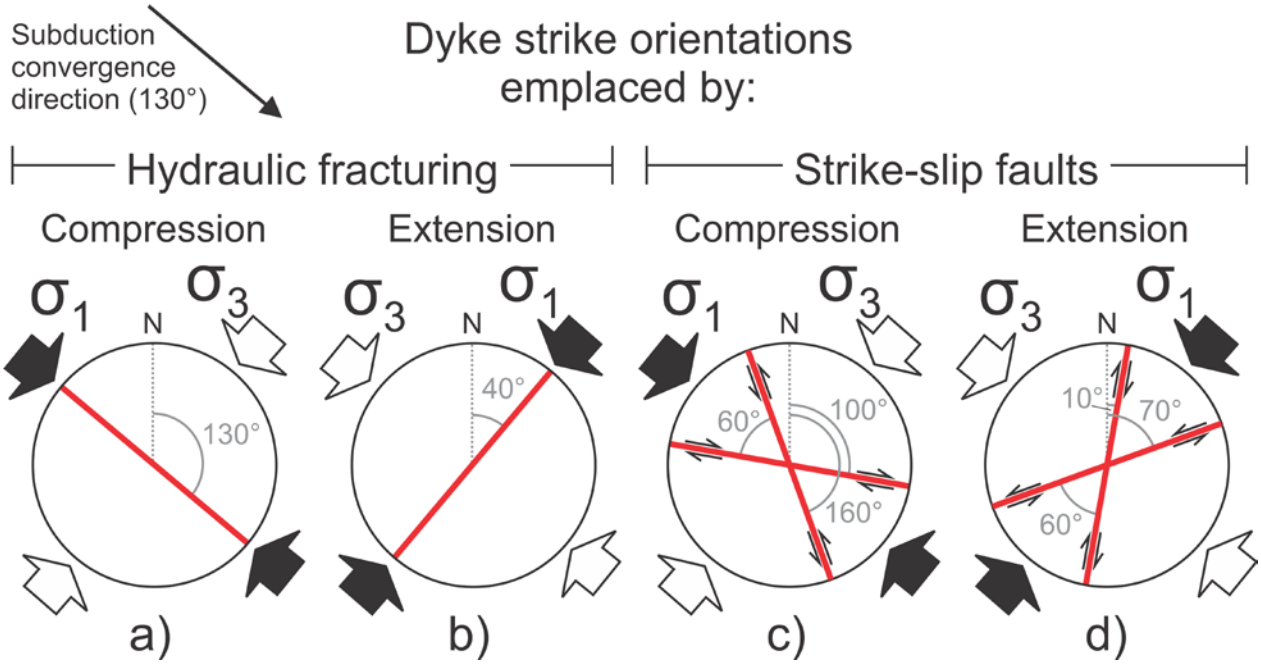

628

629 **Fig. 7.**

630 Predicted strike directions for magmatic dykes emplaced via hydraulic fracturing or by reactivation of strike-slip faults
631 during subduction-driven compression or extension of the South Shetland Islands.

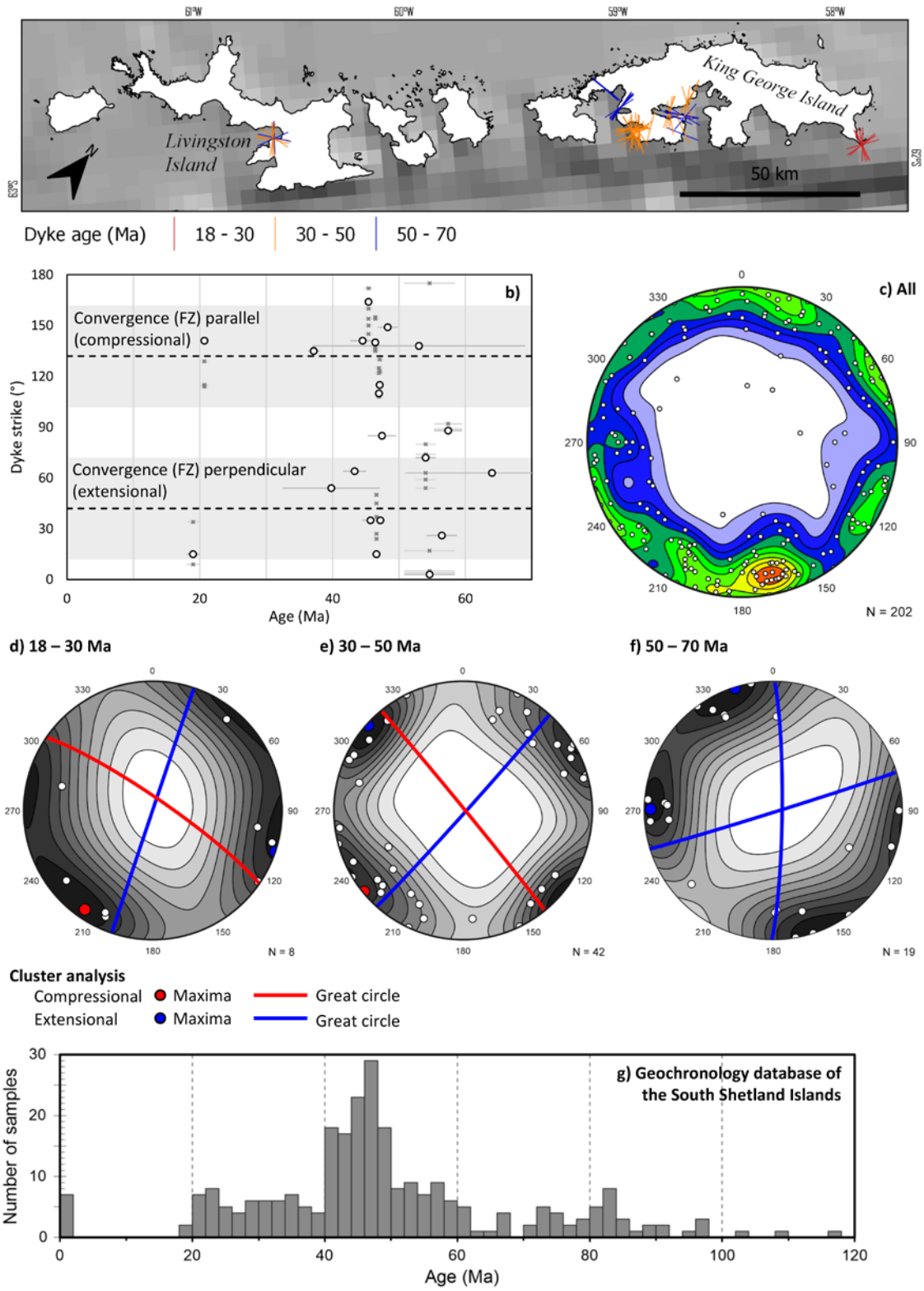

Fig. 8.

Dyke orientations of the South Shetland Islands Data. from this study, Kraus (2005), and Kraus et al. (2008, 2010). a) locations and mapped dyke orientations. b) Dyke strike directions over time (circles – directly dated sample; crosses – probable ages based on field relationships with directly dated samples). c) Poles to all dyke planes. d–f) Poles to dyke planes in 20 Ma intervals, showing the bimodal orientations during each period. g) 120–0 Ma geochronology

639 database of all analysed magmatic activity on the South Shetland Islands, selected from the database in Fig. 1
640 (Supplementary Material). Data in 2 Ma bins.

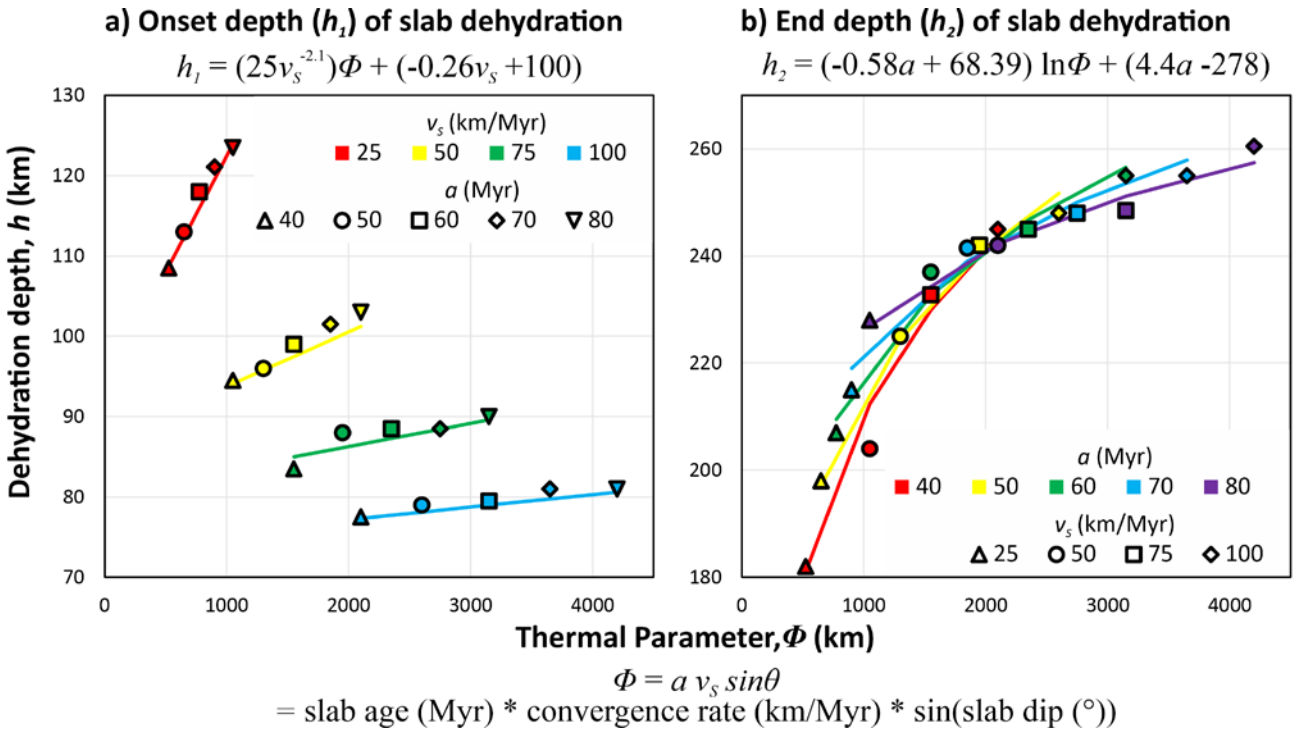

641

642 **Fig. 9.**

643 Empirical relationships between the depth and thermal parameter at the onset (a) and cessation (b) of slab dehydration,
644 plotted against the numerical modelling results of Magni et al. (2014) from which these relationships were derived.

645

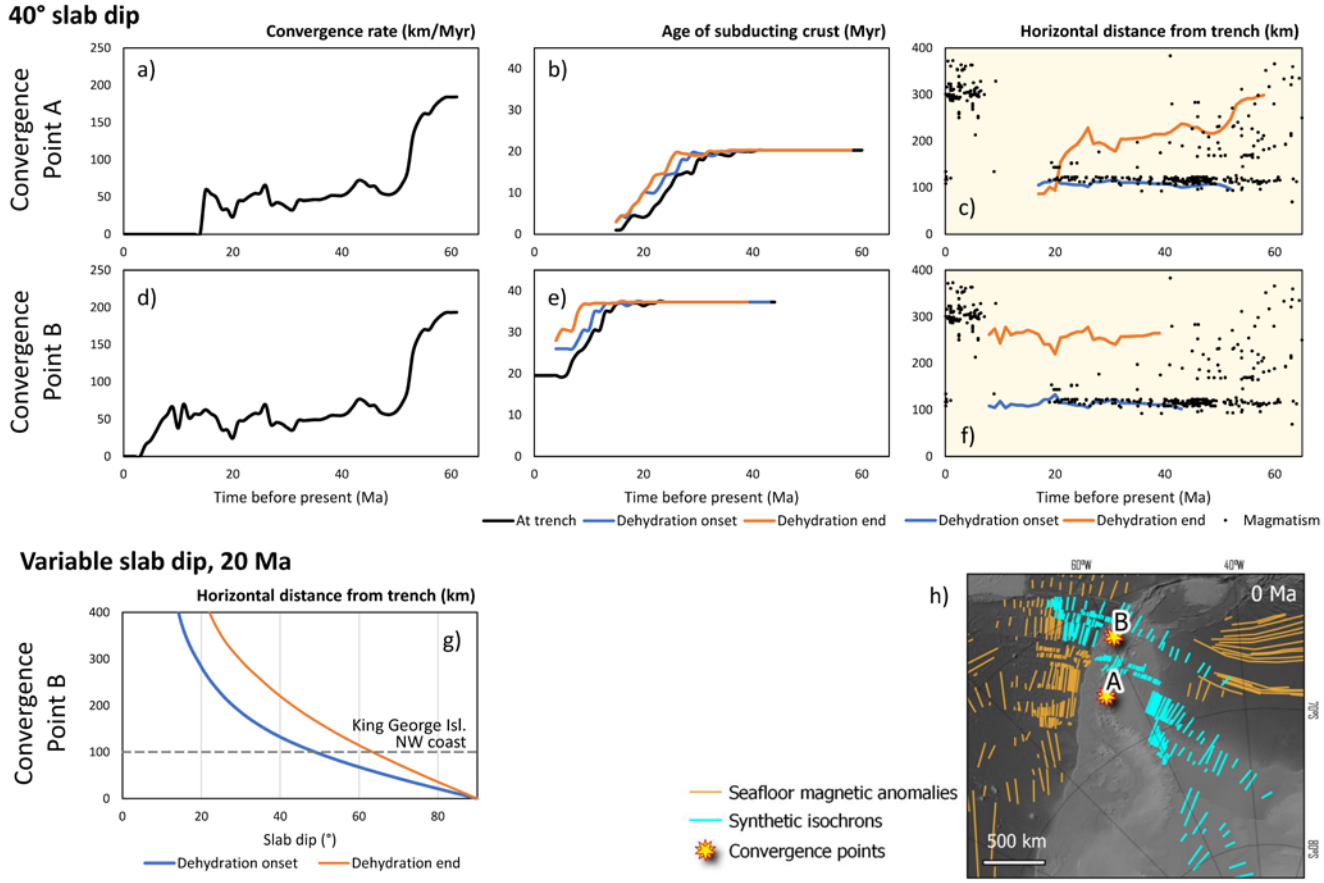

646

647 **Fig. 10.**

648 Estimating the expected width and timing of the Antarctic Peninsula magmatic arc based on the convergence rate and
649 slab age of the Phoenix Plate, and the empirical relationships of Fig. 9, calculated for convergence points A and B in
650 part 'h'. a) and d): Convergence rates between the Phoenix and Antarctic Plate. b) and e): Ages of the subducting crust
651 at the trench and its calculated onset and end dehydration depths over time. c) and f): Estimated horizontal distance of
652 slab dehydration from the trench, compared with the magmatic geochronology compilation of Fig. 5a, assuming a
653 constant 40° slab dip. g): Estimated horizontal distance from the trench of slab dehydration for convergence point B at
654 20 Ma with different slab dips. h): Marine magnetic anomalies (orange lines), synthetic isochrons of the Phoenix Plate
655 (blue lines), and locations of the convergence points.

656